

A New Modeling Method to Reveal Pumping Mechanism of Turbomolecular Pump

K. Sun, S. W. Zhang[†], F. Han, F. Zhao, Z. J. Zhang and J. Han

School of Mechanical Engineering & Automation, Northeastern University, Shenyang, Liaoning, 110819, China

[†]*Corresponding Author Email: zhangsw-neu@163.com*

(Received January 11, 2020; accepted June 8, 2020)

ABSTRACT

In order to meet the calculating requirements of high speed and miniaturized turbomolecular pump (TMP), a new modeling method is proposed for a rotor-stator row. In the same Cartesian coordinate system, the analytical equations of blade row are derived according to the real three-dimensional geometric model. A self-defining procedure is written to simulate the flow of gas molecules in TMP based on test particle Monte Carlo method. The procedure not only can calculate transmission probability of rotor row, stator row and a rotor-stator row but also evaluate the pumping performance of different blade parameters. The simulation results and known experimental data have a good agreement to confirm the feasibility of presented modeling method. The flow analysis shows that molecules at outlet of rotor row tend to accumulate in large radius and this phenomenon is obvious for high rotational speed. The differences were found between a single-stage row and a rotor-stator row. In rotor row, the molecular density at the rear blades is the highest. This is beneficial for pumping speed of TMP because 57% of molecules at the rear blades are likely to reach outlet. This will provide a direction for the structural optimization design of the blades in the future. In stator row, the molecular density reaching outlet does not significantly increase with the increase of blade velocity ratio, which indicates that the stator row is mainly used to increase the pressure ratio of TMP. The analysis of molecular density in each region reveals the pumping mechanism of TMP.

Keywords: Pumping mechanism; Flow analysis; Turbomolecular pump; Transmission probability; Rotor-stator row; Monte Carlo method.

NOMENCLATURE

A1	inlet of rotor	B6	outlet of stator
A2	front blades of rotor	b_{r_r}	stator blades root radius
A3	rear blades of rotor	b_{r_t}	stator blades tip radius
A4 (B4)	rotor body	b_{α}	stator blades angle
A6	outlet of rotor	b_h	stator blades height
A5 (B5)	casing	b_b	stator blades thickness
a_{r_r}	rotor blades root radius	b_{s_r}	stator blades spacing root
a_{r_t}	rotor blades tip radius	b_{s_t}	stator blades spacing tip
a_{α}	rotor blades angle	b_n	number of stator blades teeth
a_h	rotor blades height	M	gas molecule mass
a_b	rotor blades thickness	R	universal gas constant
a_{s_r}	rotor blades spacing root	T	temperature
a_{s_t}	rotor blades spacing tip	V_{mp}	the most probable velocity
a_n	number of rotor blades teeth		
B1	inlet of stator		
B2	front blades of stator		
B3	rear blades of stator		

1. INTRODUCTION

Turbomolecular pump (TMP) is a key apparatus for obtaining and maintaining high vacuum and ultrahigh vacuum conditions, and widely used in many fields such as semiconductor manufacturing, coating technology and high energy physics applications (Wang *et al.* 2009; Huang *et al.* 2019). In recent years, with the development of magnetic bearings (Mao and Liu 2018; Zhang *et al.* 2019), the rotational speed of TMP is getting higher and higher, and it has approached or exceeded the average thermal motion velocity of gas molecules. At this time, the pumping mechanism and performance parameters of TMP will show an obvious change. Besides, the demand for portable mass spectrometers (Chen and Lu 2019; Li *et al.* 2019; Zhou 2014) also promotes the development of TMP miniaturization, which puts higher requirements on the precise design of TMP. Thus, a new modeling method to simulate the flow of gas molecules and reveal pumping mechanism of TMP is quite necessary.

The traditional modeling method was built based on a single-stage row (a rotor row or a stator row). In the early days, Schneider *et al.* (1998) and Heo and Hwang (2000) built relatively simple geometric models. They predicted the compression ratio and speed factor of a single-stage TMP according to two dimensional (2D) models. With the widespread application of Monte Carlo methods, Chang and Jou (2001), Wang *et al.* (2009) and Li *et al.* (2014) used the three dimensional (3D) models to analysis the pumping performance of TMP by direct simulation Monte Carlo method. However, these traditional researches only calculated the performance parameters of a single-stage TMP by building a simple blade row model.

Originally, Amoli *et al.* (2004) and Hosseinalipour *et al.* (2005) started to try to carry out research on some features of molecular flow in a rotor-stator row, and considered the thickness of the blades. The numerical results had a good agreement with known experimental data by the test-particle Monte Carlo method (TPMC). But they did not make a detailed division for blade rows and did not give the solution equations for flight time of gas molecules reaching different regions. Later, Shams *et al.* (2010) compared the simulation result of the nonparallel blades with that of similar parallel blades by using TPMC method. But the blade thickness was ignored and the algorithm was not provided in detail. In addition, most studies were mainly focused on magnetic bearing, speed factor and pressure ratio, and the pumping mechanism of TMP and flight direction of gas molecules was rarely concerned.

In the present work, the whole of rotor row and stator row is respectively divided into 6 regions (boundaries) to study the flow field characteristics and flight direction of gas molecules inside the TMP. At first, we establish the 3D geometric model according to actual geometric structure of a rotor-stator row. The blade thickness is considered. Moreover, the analytical equations of blade rows

are derived in an inertial reference frame. The flight time of gas molecules from a region to other regions is solved. Finally, the number of gas molecules in each region is counted by a self-defining procedure. The procedure is written for a rotor-stator row based on TPMC method. The simulation results and published experimental data are compared. The performance parameters of blade row with blade velocity ratio, relative molecular density at A6 and molecular density of different regions are investigated by the self-defining procedure.

2. MODELING

In this section, the structure of the rotor-stator row is divided, and the real 3D geometric model is built to replace with the 2D model and single-stage model. The analysis equations of blades are derived in the same Cartesian coordinate system. The flight time of gas molecules is solved. A calculation algorithm based on flight time as a criterion is proposed. The proposed modeling method (according to a rotor-stator row) is readily extended to multi-stage TMP.

2.1 Boundary Conditions

In Fig. 1, the whole region of rotor row is divided into 6 regions by different colors, including A1-A6. Similarly, the stator row is also divided into 6 regions (B1-B6) because of the reflection effect of adjacent stator row. Thus, the solution domain becomes the cylinder region from A1 to B6.

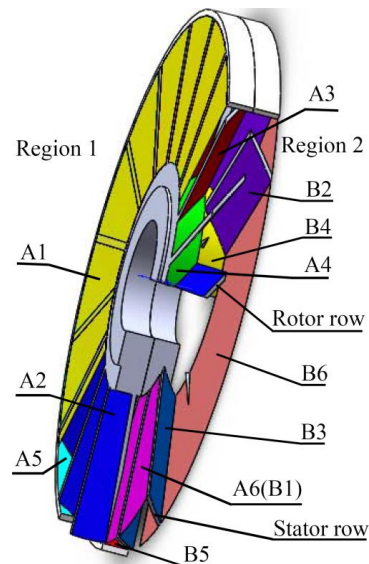


Fig. 1. Schematic diagram of the rotor row (stator row) divided into 6 regions.

A2, A3, A4 and B4 are the moving walls. The gas molecules from A2, A3, A4 and B4 have the velocity combined the tangential velocity component of the blade rotation with diffuse reflection velocity. B2, B3, B5 and A5 are the solid walls. The gas molecules from B2, B3, B5 and A5 have a diffuse reflection velocity. A1 and B1 are the inlet boundary. A6 and B6 are the outlet boundary.

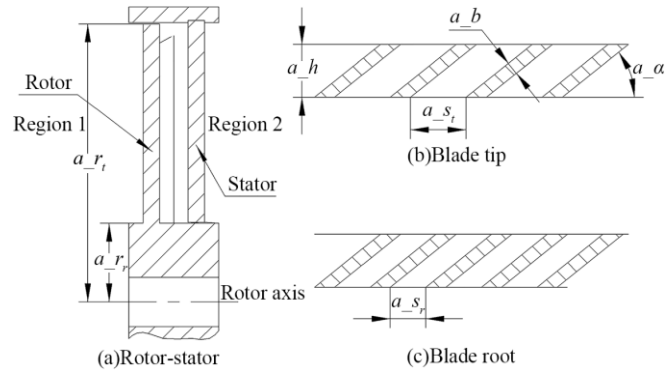


Fig. 2. Cross-sectional view of rotor-stator and rotor blades.

Figure 2 shows cross-sectional view of rotor-stator and rotor blades. In these figures, the relevant geometry is represented. Since the rotor blades and stator blades have almost the same geometry, the sectional view of stator blades is no longer given.

2.2 Analytical Equations

2.2.1 Establishing Coordinate System

Firstly, a Cartesian coordinate system (OXYZ) is established, which is stationary relative to the casing (A5 and B5). The origin O is located on the center line of the casing, and the positive direction of the X-axis is the same as the pumping direction of TMP, and the area formed by the Y-axis and the Z-axis coincides with the A1 region, as shown in Fig. 3.

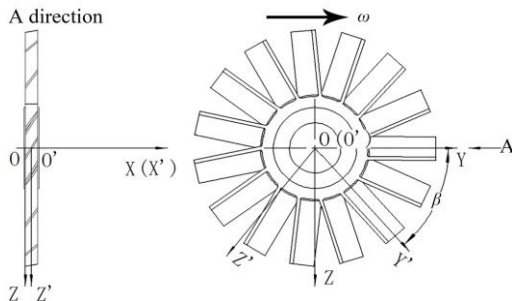


Fig. 3. Schematic diagram of relative position between rotary and stationary coordinate system.

Secondly, a rotary coordinate system O'X'Y'Z' is established, which is stationary relative to the rotor row. The blade surface extends in the direction of the radius, and the Y'-axis passes through the geometric center of one of the blades. The origin O' is located on the rotary axis of the rotor row, and the positive direction of the X'-axis is the same as the pumping direction of TMP, as shown in Fig. 3.

Finally, the coordinate transformation relationship under rotary and stationary coordinate system is obtained by Eq. (1) and Eq. (2).

$$\begin{cases} x' = x - a_h/2 \\ y' = y \cos \beta + z \sin \beta, & a_r^2 < y^2 + z^2 < a_t^2 \\ z' = z \cos \beta - y \sin \beta & 0 \leq x \leq a_h \end{cases} \quad (1)$$

$$\begin{cases} x = x' + a_h/2 \\ y = y' \cos \beta - z' \sin \beta, & a_r^2 < y'^2 + z'^2 < a_t^2 \\ z = z' \cos \beta + y' \sin \beta & -a_h/2 \leq x' \leq a_h/2 \end{cases} \quad (2)$$

where $\beta = \omega t$, ω is the angular velocity of rotor row and t is the flight time of gas molecules.

2.2.2 Analytical Equations of Blades

According to the Fig. 3, the analytical equation of the blade No. 0 in rotor row (A2 in Fig. 1) under the rotatory coordinate system can be expressed by Eq. (3).

$$\begin{cases} x' = -\left(z' + \frac{a-b}{2 \sin a_\alpha}\right) \tan a_\alpha \\ a_r \leq y' \leq a_t \\ \frac{a-b+a_h \cot a_\alpha}{2} \leq z' \leq \frac{a-b+a_h \cot a_\alpha}{2} \end{cases} \quad (3)$$

Combined with Eq. (1), under the stationary coordinate system, the A2 analytical equation of blade No. a_m in rotor row is given by Eq. (4) when the rotor rotates at an angle velocity of ω for t time. Its detailed derivation process is described in the appendix.

$$\begin{aligned} & \left(x - \frac{a-h}{2}\right) \cot a_\alpha - y \sin \left(\frac{2\pi a_m}{a_n} + \omega t\right) \\ & + z \cos \left(\frac{2\pi a_m}{a_n} + \omega t\right) + \frac{a-b}{2 \sin a_\alpha} = 0 \end{aligned} \quad (4)$$

Where a_m is blade number and it is obtained by Eq. (5).

$$a_m = \text{Int} \left(\frac{\theta}{2\pi} \cdot a_n \right), \quad 0 \leq \theta < 2\pi \quad (5)$$

Where θ is determined by the position of gas molecules, as shown in Eq. (6).

$$\theta = \begin{cases} \arccos \left(\frac{y}{\sqrt{y^2 + z^2}} \right) & a_r < y < a_t \\ & z \geq 0 \\ 2\pi - \arccos \left(\frac{y}{\sqrt{y^2 + z^2}} \right) & a_r < y < a_t \\ & z < 0 \end{cases} \quad (6)$$

Table 1 Solving equations of flight time t

Molecules in rotor row	Solving equations, $j \in [1,6]$	Molecules in stator row	Solving equations, $j \in [1,6]$
at_{j1}	x_j / v_{xj}	bt_{j1}	x_j / v_{xj}
at_{j2}	Combined Eq. (10) with Eq. (4), the flight time t is obtained.	bt_{j2}	Combined Eq. (10) with Eq. (8), the flight time t is obtained.
at_{j3}	Combined Eq. (10) with Eq. (7), the flight time t is obtained.	bt_{j3}	Combined Eq. (10) with Eq. (9), the flight time t is obtained.
at_{j4}	The surface equation of rotor body is expressed as $y^2 + z^2 = a_r r^2$. Combined Eq. (10), the flight time t is obtained.	bt_{j4}	The surface equation of rotor body is expressed as $y^2 + z^2 = b_r r^2$. Combined Eq. (10), the flight time t is obtained.
at_{j5}	The surface equation of casing is expressed as $y^2 + z^2 = a_t r^2$. Combined Eq. (10), the flight time t is obtained.	bt_{j5}	The surface equation of casing is expressed as $y^2 + z^2 = b_t r^2$. Combined Eq. (10), the flight time t is obtained.
at_{j6}	$(a-h-x_j) / v_{xj}$	bt_{j6}	$(b-h-x_j) / v_{xj}$

Similarly, the A3 analytical equation in rotor row is given by Eq. (7).

$$\left(x - \frac{a-h}{2}\right) \cot \alpha - y \sin \left(\frac{2\pi a-m}{a-n} + \omega t\right) + z \cos \left(\frac{2\pi a-m}{a-n} + \omega t\right) - \frac{a-b}{2 \sin \alpha} = 0 \quad (7)$$

Aim to the analytical equations in stator row (B2 and B3), the solving process is similar with A2 and A3 analytical equations and the blades just no longer have a rotational speed. Thus, the B2 and B3 analytical equations are respectively obtained by Eq. (8) and Eq. (9).

$$\left(x - \frac{b-h}{2}\right) \cot \alpha + y \sin \left(\frac{2\pi b-m}{b-n}\right) - z \cos \left(\frac{2\pi b-m}{b-n}\right) + \frac{b-b}{2 \sin \alpha} = 0 \quad (8)$$

$$\left(x - \frac{b-h}{2}\right) \cot \alpha + y \sin \left(\frac{2\pi b-m}{b-n}\right) - z \cos \left(\frac{2\pi b-m}{b-n}\right) - \frac{b-b}{2 \sin \alpha} = 0$$

(9) 2.2.3 Solving Flight Time

Assuming that gas molecules from j region to i region are straight lines, the motion of a molecule in Cartesian coordinate system can be expressed by Eq. (10).

$$\begin{cases} x_i = x_j + v_{xj} \cdot t \\ y_i = y_j + v_{yj} \cdot t \\ z_i = z_j + v_{zj} \cdot t \end{cases} \quad (10)$$

where $j \in [1,6]$, $i \in [1,6]$ and $j \neq i$. In Table 1, the solving equations of flight time t are given. Since

the molecules can't return to the departure regions, it can only reach the remaining 5 regions.

3. METHOD AND BASIC ASSUMPTIONS

3.1 Method

Monte Carlo method (Eskandari and Salman Nourazar 2018; Baliti *et al.* 2019; Ghatreh Samani and Meghdadi Isfahani 2019) has been applied to many fields. It can also be used to research the structure of TMP inlet (Sun *et al.* 2018, 2019). In order to accurately simulate the flight process of gas molecules in the rotor-stator row, a molecule is replaced by a particle. In this way, all molecules are tracked by test particles. This method is also regarded as the TPMC method (Tuer and Springer 1973). In this paper, TPMC method is selected to investigate the transmission probability and flow analysis of a rotor-stator row. It can reproduce the pumping process of TMP very well.

3.2 Basic Assumptions

As is known to all, the probability of gas molecules passing from upstream (Region 1 in Fig. 1) to downstream (Region 2 in Fig. 1) is the positive transmission probability Σ_{12} , and the probability from region 2 to region 1 is the reverse transmission probability Σ_{21} . It can be shown that the maximum pressure ratio (K_{\max}) and the maximum speed factor (Q_{\max}) of rotor-stator row would be solved by Eq. (11) and Eq. (12).

K_{\max} and Q_{\max} are two important performance characteristics of TMP (Wang *et al.* 2009).

$$K_{\max} = \Sigma_{12} / \Sigma_{21} \quad (11)$$

$$Q_{\max} = \Sigma_{12} - \Sigma_{21} \quad (12)$$

When calculating Σ_{12} , a uniform distribution of gas molecules at A1 is assumed. The initial position of a molecule in Cartesian coordinate system can be given in terms of random number (R_f) by Eq. (13). The molecules obey Maxwellian velocity distribution at A1. The initial velocity is generated by Eq. (14).

$$\begin{cases} x_0=0 \\ y_0=\sqrt{a_{-r_r}^2+R_f(a_{-r_t}^2-a_{-r_r}^2)}, 0 < R_f < 1 \\ z_0=\sqrt{a_{-r_r}^2+R_f(a_{-r_t}^2-a_{-r_r}^2)} \end{cases} \quad (13)$$

$$\begin{cases} v_{x0}=\sqrt{-\ln R_f} V_{mp} \\ v_{y0}=\sqrt{-\ln R_f} V_{mp} \cos(2\pi R_f) \\ v_{z0}=\sqrt{-\ln R_f} V_{mp} \sin(2\pi R_f) \end{cases} \quad (14)$$

Where the most probable velocity $V_{mp}=\sqrt{2RT/M}$. When calculating Σ_{21} , the molecules are generated at B6. The x_0 initial position and the v_{x0} initial velocity need to be changed with $x_0=b-h$ and $v_{x0}=-\sqrt{-\ln R_f} V_{mp}$, respectively. Other parameters remain unchanged.

A diffusive collision model is assumed when the molecules collide with the walls. The shortest flight time to each region is regard as a criterion that determines the position of molecules collision with the wall. According to the position of the collision, the number of molecules colliding in each region can be counted.

4. VERIFICATION OF MODEL

A self-defining procedure was written based on the new modeling method. In order to verify the feasibility of the procedure, the simulation results were compared with the published experimental data (Sawada *et al.* 1971) and the geometric parameters of blades are given in Table 2.

In Fig. 4, it is easy to find that the initial simulation results have some errors with the experimental results. This is caused by initial model ignoring the clearance between the blades tip and the casing. In the paper of Wang *et al.* (2009), the effect of clearance on the maximum pressure ratio was studied. Compared with the actual model, the maximum pressure ratio of the model without clearance is larger about 8%. So the correction coefficient is introduced to make up for the shortage of the simplified model in this paper. The modified simulation results have a good agreement with the experimental results when the blade velocity ratio $c < 1$ ($c = \pi\omega(a_{-r_r}+a_{-r_t})/V_{mp}$). When $c > 1$,

the increase in the maximum pressure ratio is gradually stable. This is different from the previous calculation theory (Amoli and Hosseinalipour 2004) that the relationship between the maximum pressure ratio and the blade velocity ratio is exponential

function. The possible cause is that gas molecules have reached saturation point when TMP is at high rotational speed. Thus, it is inadvisable to increase the pressure ratio by simply increasing the rotational speed without changing the blade row structure. The performance test of TMP at high rotational speed is under construction. This research work is also in line with the current calculating demand for high rotational speed of TMP.

Table 2 Geometric parameters of rotor row (Stator is the same as rotor)

Notations	Unit	Blade No.1	Blade No.2	Blade No.3
a_{-r_r}	mm	72	72	72
a_{-r_t}	mm	90	90	90
$a_{-\alpha}$	°	20	30	40
a_{-h}	mm	8	8	8
a_{-b}	mm	3.2	3.1	2.9
a_{-s_r}	mm	9.5	6.4	4.9
a_{-s_t}	mm	14.3	9.5	7.2
a_{-n}	—	24	36	48

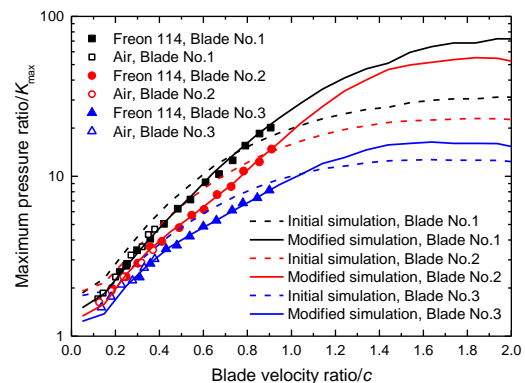


Fig. 4. Variation of maximum pressure ratio as blade velocity ratio for rotor-stator with different blade parameters.

5. RESULTS

5.1 Pumping Performance

The variation of performance parameters with blade velocity ratio is calculated by the self-defining procedure. The structural parameters of blade No. 2 are selected to study pumping performance. With the increase of the rotational speed, Σ_{12} of rotor row and of stator row gradually increase, but Σ_{21} of them gradually decreases from Fig. 5. The maximum speed factor and maximum pressure ratio all increase with blade velocity ratio from Fig. 6. This is in accordance with the actual theory that the pumping speed and pressure ratio of TMP increase with the increase of the rotational speed. If the transmission probability of a stator row is calculated

independently, the results of Σ_{12} and Σ_{21} should be equal. Actually, Σ_{12} and Σ_{21} of a stator row is unequal (as shown in Fig. 5) when considering a rotor-stator row. So the modeling method of a rotor-stator row is more reasonable in the paper.

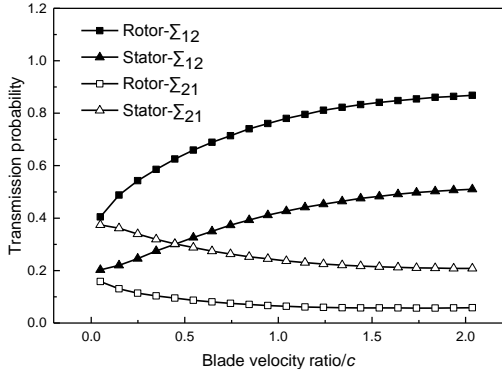


Fig. 5. Change in transmission probability of rotor and stator with blade velocity ratio.

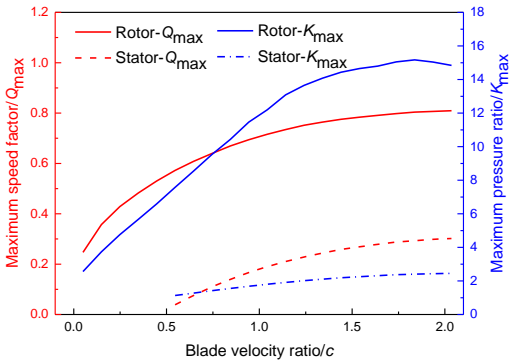


Fig. 6. Change in performance parameters of rotor and stator with blade velocity ratio.

In Fig. 5, Σ_{12} of rotor row is larger than that of stator row, but Σ_{21} of rotor row is smaller than that of stator row. The former indicates that the stator row acts to increase the pressure ratio, and the latter illustrates that the rotor row reduce the backflow because the small transmission probability hinders the transmission of gas molecules. This also explains why the blades inside TMP need alternate arrangement of rotor row and stator row.

5.2 Relative Molecular Density at A6

Figure 7 shows the variation of relative molecular density $E(r)$ at A6 versus non-dimensional radius r/a_{-r} when the blade velocity ratio (based on rotor mean radius) is 0.5, 1.0, 1.5 and 2.0. The relative molecular density $E(r)$ is calculated by Eq. (15). The uniform density distribution $E_{UDD}(r)$ curve can be obtained by Eq. (16).

$$E(r) = \frac{N_r}{N_{A6}} \quad (15)$$

$$E_{UDD}(r) = \frac{S_r}{S_{A6}} \quad (16)$$

where N_r and S_r are the partial molecular number and the partial annular area at radius r , respectively. N_{A6} and S_{A6} are the total molecular number and the entire annular area at A6 region, as shown in Fig. 8.

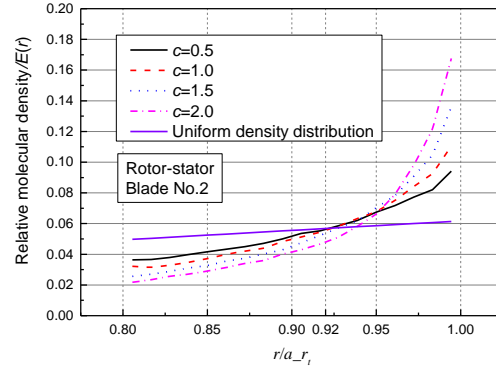


Fig. 7. Relative molecular density at A6.

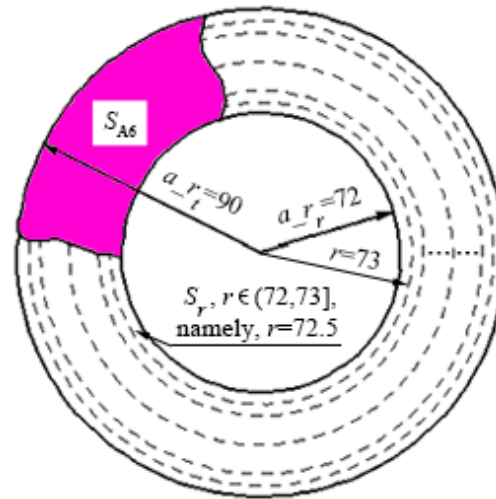


Fig. 8. Sketch of relevant parameters definition about molecular density at A6.

The A6 is divided into 18 intervals according to 1mm as a annular area and the annular area radius is represented by the average radius (For example, $r \in (72\text{mm}, 73\text{mm}]$ is regard as $r = 72.5\text{mm}$). The calculation results indicate that the molecules accumulate in large radius, as shown in Fig. 7. The higher the rotational speed is, the more significant the aggregation effect is, which is mainly because the molecules from rotor row are tangential velocity. This phenomenon is consistent with that found by Amoli *et al.* (2004).

When r/a_{-r} is approximately equal to 0.92, the curve of uniform density distribution intersects the other curves. In this position, the relative molecular density is just uniform distribution. This indicates that the most gas molecules passing rotor row are

not uniform distribution. In other words, it was unscientific to regard the gas molecules before entering stator row as a uniform distribution in the past.

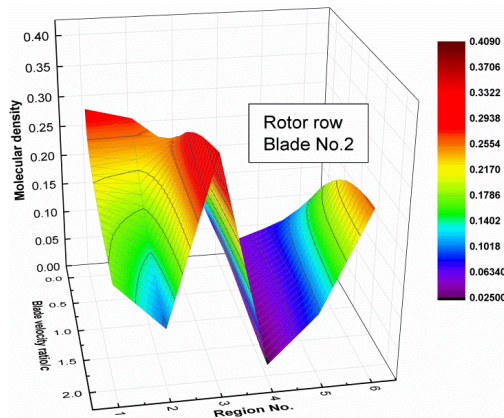


Fig. 9. Cloud chart of molecular density with blade velocity ratio at A1~A6 for rotor row.

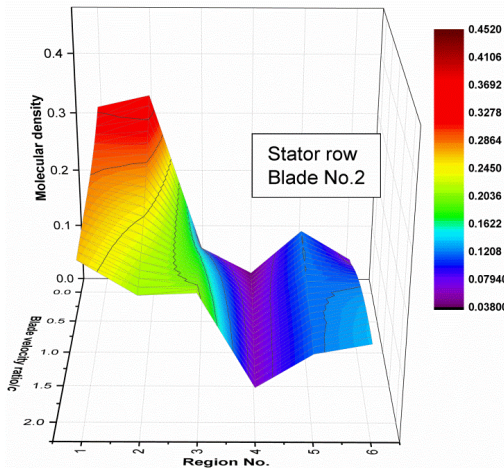


Fig. 10. Cloud chart of molecular density with blade velocity ratio at B1~B6 for stator row.

5.3 Molecular Density for Different Regions

Figures 9 and 10 show the cloud chart of molecular density with blade velocity ratio at A1~A6 for rotor row and at B1~B6 for stator row, respectively. They are helpful to analyze the movement tendency of gas molecules in the rotor and stator blades and provide the research direction of improving the performance of TMP. For example, in Fig. 9, it is found that the variation trend of molecular density at A3 with the blade velocity ratio is the same as that of A6. This suggests that increasing the molecular density at A3 can increase the number of molecules reaching A6, so as to increase the pumping speed of TMP. Again as in Fig. 10, the molecular density at B1 and B2 is relatively high. With the increase of the rotational speed, however, the molecular density at B6 does not increase significantly. This indicates that the stator row mainly plays a role in increasing the

pressure ratio in TMP because gas pressure is proportional to molecular density. Based on this algorithm and analysis method, the performance of TMP should be improved and optimized by changing the structural parameters of the rotor and stator blades in the future.

Whether in rotor row or in stator row, the molecular density at A5 (B5) is always higher than that of A4 (B4), which is consistent with the phenomenon of molecules tending to collect in large radius. It is not difficult to find that with the increase of the rotational speed, the molecular density at A3 (B3) increases and the molecular density at A2 (B2) decreases. In rotor row (based on blade No.2), since the 57% of the molecules reflected from A3 are possible to reach A6, the results conform to the characteristic that the pumping speed of TMP becomes greater with the increase of the rotational speed. Figures 9 and 10 reveal the pumping mechanism of TMP in more detail. The molecular density of each region in rotor-stator row is given from the perspective of molecular gas dynamics. This will be a good help for the next step in blades structural design.

6. CONCLUSION

A new theoretical modeling method of the simulation analysis for TMP is put forward. The pumping characteristic of a rotor-stator row in molecular flow region is investigated based on TPMC method. A quite good agreement between modified simulation results and experimental data confirms the feasibility of the self-defining procedure. The procedure that proposed in this paper for a rotor-stator row can be readily extended to multi-stage TMP and calculate the pumping performance of different blade structure parameters.

According to the example given in this paper, the following conclusions are obtained.

- (1) For rotor row and stator row, the variation of transmission probability with blade velocity ratio explains the reason that the blades inside TMP need alternate arrangement of rotor row and stator row.
- (2) The flow analysis at A6 shows that the molecules tend to collect in large radius and this phenomenon is obvious for high blade velocity ratio. It shows that the gas molecules reaching B1 region are no longer evenly distributed.
- (3) In cloud chart of rotor row, the molecular density at A3 is the highest. This is beneficial for pumping speed of TMP because 57% of the molecules at A3 are likely to reach A6 (based on $c=1$ and blade No.2). This will provide a direction for future structural design.
- (4) In cloud chart of stator row, the molecular density at B6 does not increase significantly with the increase of blade velocity ratio, which indicates that the stator row is mainly used to increase the pressure ratio of TMP.

The above analysis also reveals the pumping mechanism of TMP from the perspective of molecular gas dynamics. The new theoretical model solves the problem of inaccurate calculation of high speed and miniaturized TMP in the past. Based on the proposed modeling method, the calculation of multi-stage TMP and the optimization of blade structure parameters will be performed in the next stage. And the experimental research will also be carried out by referring to the simulation results.

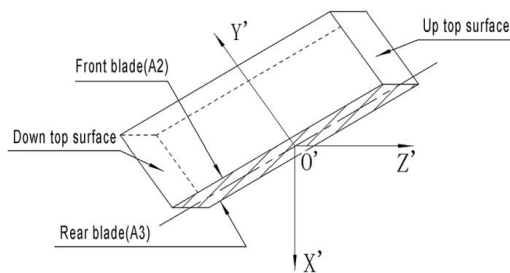


Fig. 11. Schematic diagram of a blade in the rotary coordinate system.

APPENDIX

The analytical equation of the blade is very important during the simulation calculation process. It is directly related to the accuracy of the calculation results. The analytical equation of the front blades (A2) is selected under the stationary coordinate system, as shown in Eq. (4). Its derivation process is as follows.

In Fig. 11, the analytical equation of front blade (A2) is easily obtained under the rotatory coordinate system, as shown in Eq. (3). It needs to be converted to a stationary coordinate system because the analytical equations of rotor row and stator row should be under the same coordinate system.

Combined with Eq. (1) ($x' = x - a_h/2$ and $z' = z \cos \beta - y \sin \beta$), Eq. (3) can be expressed as follows:

$$\left(x - \frac{a_h}{2}\right) \cot \alpha - y \sin \beta + z \cos \beta + \frac{a_b}{2 \sin \alpha} = 0 \quad (17)$$

Eq. (17) is only the analytical equation of the blade No. 0 when the rotor rotates at an angle velocity of ω for t time. If blade No. a_m represents any blade number, the A2 analytical equation of blade No. a_m is obtained by Eq. (4) when the rotor rotates at an angle velocity of ω for t time, as shown in Eq. (18).

$$\left(x - \frac{a_h}{2}\right) \cot \alpha - y \sin \left(\frac{2\pi a_m}{a_n} + \omega t\right) + z \cos \left(\frac{2\pi a_m}{a_n} + \omega t\right) + \frac{a_b}{2 \sin \alpha} = 0 \quad (18)$$

The derivation processes of Eq. (7), Eq. (8) and Eq.

(9) are similar with Eq. (4). Thus, their solution process is no longer given in appendix.

REFERENCES

- Amoli, A. and S. M. Hosseinalipour (2004). A continuum model for pumping performance of turbomolecular pumps in all flow regimes. *Vacuum* 75(4), 361-366.
- Amoli, A., R. Ebrahimi and S. M. Hosseinalipour (2004). Some features of molecular flow in a rotor-stator row with real topology. *Vacuum* 72(4), 427-438.
- Baliti, J., M. Hssikou and M. Alaoui (2019). Gas Flow and Heat Transfer in an Enclosure Induced by a Sinusoidal Temperature. *Journal of Applied Fluid Mechanics* 12(6), 1757-1767.
- Chang, Y. W. and R. Y. Jou (2001). Direct simulation of pumping characteristics in a fully 3D model of a single-stage turbomolecular pump. *Applied Surface Science* 169-170, 772-776.
- Chen, Y. H. and I. C. Lu (2019). Novel ion source for a portable mass spectrometer. *Rapid Communications in Mass Spectrometry*, 1-5.
- Eskandari, M. and S. Salman Nourazar (2018). On the Expedient Solution of the Boltzmann Equation by Modified Time Relaxed Monte Carlo (MTRMC) Method. *Journal of Applied Fluid Mechanics* 11(3), 655-666.
- Ghatreh Samani, S. and A. H. Meghdadi Isfahani (2019). A New Relaxation Time Model for Lattice Boltzmann Simulation of Nano Couette Flows in Wide Range of Flow Regimes. *Journal of Applied Fluid Mechanics* 12(6), 1781-1790.
- Heo, J. S. and Y. K. Hwang (2000). DSMC calculations of blade rows of a turbomolecular pump in the molecular and transition flow regions. *Vacuum* 56(2), 133-142.
- Hosseinalipour, S. M., R. Ebrahimi and A. Amoli (2005). A new procedure for designing blade arrangements of a turbomolecular pump. *Rarefied Gas Dynamics* 762, 186-191.
- Huang, Z. Y., Han, B. C. and Y. Le (2019). Multidisciplinary Design Strategies for Turbomolecular Pumps With Ultrahigh Vacuum Performance. *Ieee Transactions on Industrial Electronics* 66(12), 9549-9558.
- Li, X. X., Y. J. Zhang, S. J. Ge, J. Qian and W. Miao (2019). Portable linear ion trap mass spectrometer with compact multistage vacuum system and continuous atmospheric pressure interface. *Analyst* 144(17), 5127-5135.
- Li, Y. W., X. K. Chen, W. J. Guo, D. M. Li, Q. F. Wang and K. Feng (2014). Accurate simulation of turbomolecular pumps with modified algorithm by 3D direct simulation Monte Carlo method. *Vacuum* 109, 354-359.

- Mao, K. and G. Liu (2018). An improved braking control method for the magnetically levitated TMP with a fast transient response. *Vacuum* 148, 312-318.
- Sawada, T., M. Suzuki and O. Taniguchi (1971). The axial flow molecular pump, 2nd report. *Bulletin of JSME* 14(67), 48-57.
- Schneider, T. N., S. Katsimichas, C. R. E. de Oliveira and A. J. H. Goddard (1998). Empirical and numerical calculations in two dimensions for predicting the performance of a single stage turbomolecular pump. *Journal of Vacuum Science & Technology a-Vacuum Surfaces and Films* 16(1), 175-180.
- Shams, M., H. Sheykhzadeh and M. Taghavi (2010). Mathematical Simulation of Free Molecular Flow in a Three-Dimensional Turbomolecular Pump with Nonparallel Blades. *Journal of Dispersion Science and Technology* 31(3), 299-306.
- Sun, K., S. W. Zhang, F. Zhao, Z. J. Zhang, S. Li and Q. Z. Li (2019). A novel conical reflector and arc transition tube of turbomolecular pump. *Journal of Instrumentation* 14(06), T06007-T06007.
- Sun, K., S. Zhang, Y. Li, Z. Zhang, H. Li and R. Mu (2018). Monte Carlo simulation of gas free molecular flow in turbo molecular pump's inlet tube. *Molecular Simulation* 44(15), 1261-1269.
- Tuer, T. W. and G. S. Springer (1973). A test particle Monte Carlo method. *Computers & Fluids* 1(4), 399-417.
- Wang, S., H. Ninokata, E. Merzari, K. B. Lei, X. L. Luo, L. Y. Lu and K. Kase (2009). Numerical study of a single blade row in turbomolecular pump. *Vacuum* 83(8), 1106-1117.
- Zhang, X., B. C. Han, X. Liu, Y. L. Chen and L. X. Zhai (2019). Prediction and experiment of DC-bias iron loss in radial magnetic bearing for a small scale turbomolecular pump. *Vacuum* 163, 224-235.
- Zhou, H. L. (2014). Research on miniature mass spectrometer. *Chinese Instrumentation Technology* (4), 1-6.